Zinc chlorins for artificial light-harvesting self-assemble into antiparallel stacks forming a microcrystalline solid-state material

Ganapathy, S.; Sengupta, S.; Wawrzyniak, P.K.; Huber, V.; Buda, F.; Baumeister, U.; ... ; Groot, H.J.M. de

Zinc chlorins for artificial light-harvesting self-assemble into antiparallel stacks forming a microcrystalline solid-state material

Swapna Ganapathy[a], Sanchita Sengupta[b], Piotr K. Wawrzyniak[a], Valerie Huber[b], Francesco Buda[a], Ute Baumeister[c], Frank Würthner[b,1], and Huub J. M. de Groot[a,1]

[a]Leiden Institute of Chemistry, Einsteinweg 55, 2333CC Leiden, The Netherlands; [b]Institut für Organische Chemie, Universität Würzburg, Am Hubland, 97074 Würzburg Germany; and [c]Institut für Chemie, Martin-Luther-Universität Halle-Wittenberg, Mühlpforte 1, 06108 Halle, Germany

Edited by Michael R. Wasielewski, Northwestern University, Evanston, IL, and accepted by the Editorial Board May 21, 2009 (received for review November 21, 2008)

We introduce a concept to solve the structure of a microcrystalline material in the solid-state at natural abundance without access to distance constraints, using magic angle spinning (MAS) NMR spectroscopy in conjunction with X-ray powder diffraction and DFT calculations. The method is applied to a novel class of materials that form (semi)conductive 1D wires for supramolecular electronics and artificial light-harvesting. The zinc chlorins 3-devinyl-3^1-hydroxymethyl-13^2-demethoxycarbonylpheophorbide a (3′,5′-bis-dodecyloxy)benzyl ester zinc complex 1 and 3-devinyl-3^1-methoxymethyl-13^2-demethoxycarbonylpheophorbide a (3′,5′-bis-dodecyloxy)benzyl ester zinc complex 2, self-assemble into extended excitonically coupled chromophore stacks. ^{1}H-^{13}C heteronuclear dipolar correlation MAS NMR experiments provided the ^{1}H resonance assignment of the chlorin rings that allowed accurate probing of ring currents related to the stacking of macrocycles. DFT ring-current shift calculations revealed that both chlorins self-assemble in antiparallel π-stacks in planar layers in the solid-state. Concomitantly, X-ray powder diffraction measurements for chlorin 2 at 80 °C revealed a 3D lattice for the mesoscale packing that matches molecular mechanics optimized aggregate models. For chlorin 2 the stacks alternate with a periodicity of 0.68 nm and a 3D unit cell with an approximate volume of 6.28 nm^3 containing 4 molecules, which is consistent with space group $P2_122_1$.

artificial antenna | density functional theory | microcrystalline structure | solid state NMR | X-ray diffraction

Green sulfur bacteria and the green nonsulfur bacteria are found in anoxic environments where the light intensities can be extremely low; with single chlorophyll photon absorption rates <1 photon per hour. To survive under such low light intensities, green bacteria such as *Chlorobium tepidum* evolved chlorosomes, very efficient extramembraneous antenna systems that consist of 1–2 × 10^5 (1–3) self-organized bacteriochlorophyll (BChl) molecules in highly ordered suprastructures. Chlorosomes accomplish ultrafast energy transfer via pigment-pigment interactions, instead of pigment-protein interactions. They have the longest exciton diffusion lengths of any known pigment assembly at room temperature (4–6). The extremely fast exciton mobility leads to favorable light-harvesting efficiencies of these systems, which recommends these aggregates for possible applications in supramolecular photonic, electronic or photocatalytic devices for molecular electronics or solar energy conversion (7, 8).

It is known that the self-assembly of BChl *c* pigments observed in chlorosomes is replicated by BChl *c* aggregates in nonpolar solvents like hexane (9–11). Tamiaki and coworkers developed a model zinc chlorin compound, which is a BChl *d* analogue that forms extended dye aggregates and replicates the aggregation behavior of BChl *c* in nonpolar solvents (12). In recent years, some of us have demonstrated that the self-assembly process of BChl *c*, *d*, and *e* into a tubular structure can be mimicked by using semisynthetic zinc chlorin **1** (Fig. 1) molecules that are preprogrammed for this mode of self-assembly, i.e., possessing the 3^1-OH group, a central metal ion, and 13^{1}C═O moieties along the Q_y axis, and containing at least 2 extended alkyl tails at the 17^2 carboxylic acid substituent (13). In addition, self-assembly of highly ordered 1-dimensional (1D) π-stacks of zinc chlorin **2** (Fig. 1), with the OH substituted by a methoxy functionality, was observed by scanning tunneling microscopy (STM) on conductive and atomically flat highly oriented pyrolytic graphite (HOPG) surfaces (14).

Hence, detailed spectroscopic and microscopic investigations have already provided convincing evidence for the formation of extended π-stacks of these chromophores in solution and on surfaces (14). However, a detailed local crystal structure to elucidate the packing of the zinc chlorins (hereafter chlorin) **1** and **2** in bulk is hitherto unknown. The packing behavior of these dyes in the solid state is of importance considering the potential use of such closely spaced 1D π-stacks and layered assemblies in organic electronics and photovoltaics. Suitable single crystals for a complete X-ray crystal structure analysis are not available for these microcrystalline materials, which led us to explore the utilization of solid-state NMR in combination with powder diffraction, molecular modeling and DFT calculations to provide information about the 3D packing of the chromophores in the bulk.

Recently, MAS NMR has been successfully developed and used for structure determination of uniformly enriched compounds or multiple spin clusters in solid type biological systems, disordered systems, and polypeptides. It has been used in ^{13}C and ^{15}N enriched samples to study the self-organization of BChls in chlorosomal light harvesting antennae (11, 15). Labeling of the semisynthetic chlorins containing isotope atoms is possible using ^{13}C and ^{15}N enriched starting materials. However, materials research critically depends on the preparation and screening of multiple compounds for realizing artificial systems with the desired properties. Considering the high costs that labeled starting materials demand, this would be an expensive endeavor, because a large fraction of the labeled material is lost in a multistep synthesis or derivatization process. In such cases it is more practical and economical to have a method to screen

Author contributions: F.W. and H.J.M.d.G. designed research; S.G., S.S., P.K.W., V.H., F.B., and U.B. performed research; S.G. and U.B. analyzed data; and S.G., S.S., F.W., and H.J.M.d.G. wrote the paper.

The authors declare no conflict of interest.

This article is a PNAS Direct Submission. M.K.W. is a guest editor invited by the Editorial Board.

Freely available online through the PNAS open access option.

[1]To whom correspondence may be addressed. E-mail: wuerthner@chemie.uni-wuerzburg.de or groot_h@lic.leidenuniv.nl.

This article contains supporting information online at www.pnas.org/cgi/content/full/0811872106/DCSupplemental.

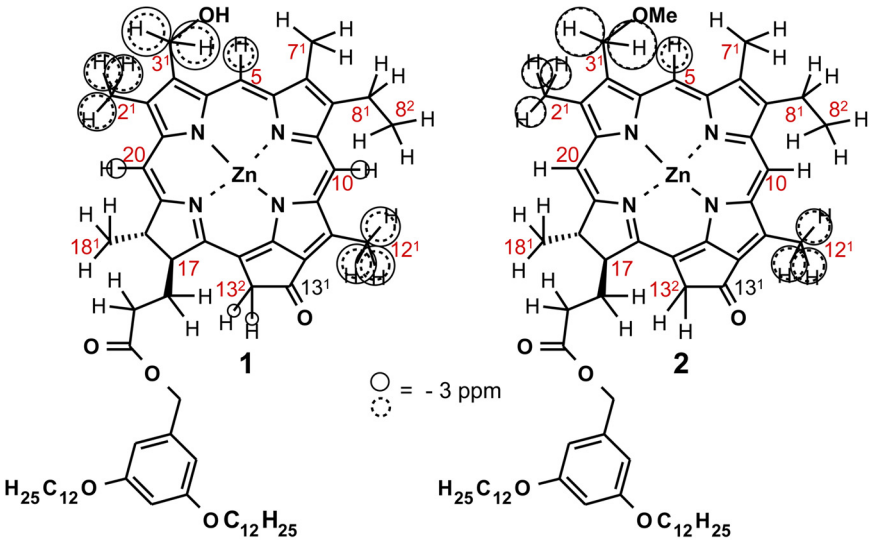

Fig. 1. Chemical structure of 3^1-hydroxy and 3^1-methoxy zinc chlorins **1** and **2**. Detected ^{1}H upfield aggregation shifts of aggregated chlorins **1** and **2** relative to their monomers in THF-d_8 and pyridine-d_5, respectively, are shown as solid circles. Calculated ring-current shifts for **1** and **2** in the antiparallel stack model are shown as dashed circles. Values less than −2 ppm are depicted. The circles have a radius proportional to the magnitude of the shift.

unlabeled compounds so as to scrutinize a large number of compounds spanning every step of the supramolecular chemical design process.

To resolve the structural arrangement of the model systems using MAS NMR combined with molecular modeling and ring current shift calculations for the unlabeled chlorin dyes, the ^{1}H shifts are first resolved using 2D heteronuclear ^{1}H-^{13}C dipolar correlation experiments and thereby the proton aggregation shifts are determined. For the highly ordered and closely spaced stacks of **1** and **2**, all of the resonances of the chlorin macrocycle can be assigned and analyzed to resolve the microstructure. This is possible because the building blocks **1** and **2** are moderately sized, unsaturated molecules of low symmetry. Access to the proton chemical shifts of aggregated chlorins allows accurate probing of ring-current effects that can be related to the stacking of macrocycles, via the chemical structure of the molecule. The unsaturation leads to a favorable dispersion of NMR signals and resolved ^{1}H-^{13}C cross peaks in the 2D spectra. Quantum mechanical calculations are then performed to quantitatively reproduce the observed ring currents. The low symmetry promotes a good accuracy of the DFT ring current analyses, because side chains are in unique positions in terms of overlap with adjacent molecules in the structure. In this way, the combination of MAS NMR, molecular modeling and DFT based ring current shift calculations provides a quantitative basis to determine the stacking patterns that chlorins **1** and **2** adopt at a molecular level. Complimentary X-ray diffraction data for chlorin **2** provide a packing model of these dyes in the solid state that substantiates this 3-dimensional organization of the chlorin subunits. Both compounds form solids with antiparallel monomer stacking, which was not yet encountered for BChl in chlorosomes. Because chlorosomes are heterogeneous and are present in different forms across a number of species, it is possible that antiparallel monomer stacking is present in nature as well.

Results and Discussion

For the assignment of the ^{1}H shifts, the FSLG technique was applied to solid samples of chlorins **1** and **2** (16). Fig. 2 shows the 2D heteronuclear ^{1}H-^{13}C spectrum where the assignment is indicated. It was possible to assign almost all of the proton resonances corresponding to the chlorin ring unambiguously for compounds **1** and **2** as depicted in Fig. 2 *A–D*. A single set of peaks without significant broadening is detected for **1** and **2**, which implies a local packing order with unique structural environments for every molecule. The 3^1-OH and 3^1-OCH_3 resonances for chlorins **1** and **2** respectively, were not observed even at lower contour levels, possibly because of some form of dynamics and inefficient cross-polarization (11, 17). The solid-state proton shift values have been listed in Table 1 as $\sigma^H_{1,i}$ and $\sigma^H_{2,i}$ respectively.

Aggregation shifts are defined as chemical shifts in the solid relative to the monomer shifts in solution. To obtain these monomer shifts, chlorin dyes **1** and **2** were dissolved in the coordinating solvents tetrahydrofuran-d_8 (THF-d_8) and pyridine-d_5, respectively. The ^{1}H monomer shifts for **1** and **2** are listed in Table 1 as $\sigma^H_{1,\mathrm{liq}}$ and $\sigma^H_{2,\mathrm{liq}}$ respectively. The aggregation shifts for **1** and **2** given by $\Delta\sigma^H_i = \sigma^H_i - \sigma^H_{\mathrm{liq}}$ are listed in Table 1. Significant upfield aggregation shifts are observed, both for chlorins **1** and **2** and these have been depicted as circles for values less than −2 ppm in Fig. 1, where the circles have a radius proportional to the magnitude of shift.

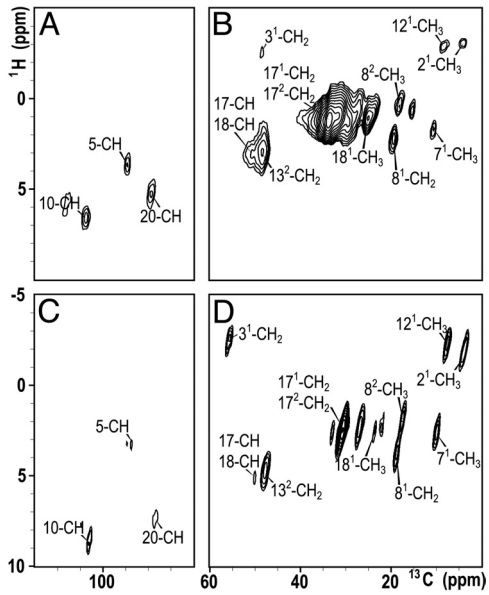

Fig. 2. Contour plot sections of ^{1}H-^{13}C heteronuclear MAS NMR dipolar correlation spectra of chlorins **1** (*A* and *B*) and **2** (*C* and *D*) recorded at a field of 17.6 T employing a spinning rate of 13 kHz and sample temperatures of 298 K. The assignments of the chlorin rings are indicated.

Table 1. ^{1}H solution (σ^H_{liq}) and experimental solid-state chemical shifts (σ^H_i) of chlorins 1 and 2, and their aggregation shifts $\Delta\sigma^H_i = \sigma^H_i - \sigma^H_{liq}$ in parts per million

Position	$\sigma^H_{1,i}$	$\sigma^H_{1,liq}$	$\Delta\sigma^H_{1,i}$	$\sigma^H_{2,i}$	$\sigma^H_{2,liq}$	$\Delta\sigma^H_{2,i}$
5	3.7	9.5	−5.8	3.3	9.3	−6.0
10	6.6	9.6	−3.0	8.8	9.6	−0.8
17	3.1	4.3	−1.2	5.1	4.2	0.9
18	3.1	4.5	−1.4	5.1	4.4	0.7
20	5.3	8.5	−3.2	7.4	8.4	−1.0
2^1	−3.1	3.3	−6.4	−1.8	3.3	−5.1
3^1	−2.5	5.7	−8.2	−2.6	5.6	−8.2
7^1	1.7	3.3	−1.6	2.6	3.3	−0.7
8^1	2.2	3.8	−1.6	3.8	3.7	0.1
8^2	0.4	1.7	−1.3	2.0	1.7	0.3
12^1	−2.9	3.7	−6.6	−2.3	3.7	−6.0
13^2	3.0	5.1	−2.1	4.7	5.1	−0.4
17^1	1.2	2.3	−1.1	2.4	1.9	0.5
17^2	1.2	2.3	−1.1	2.4	1.9	0.5
18^1	1.1	1.8	−0.7	2.4	1.7	0.7

From a correlation plot comparing the solid state chemical shifts of **1** and **2** with their monomer shifts in solution, it is clear how pronounced the ^{1}H aggregation shifts are within the ^{1}H chemical shift range (Fig. S1). The ^{1}H aggregation shifts are dominated by ring-current effects, in line with observations in other chlorin aggregates and are more useful than the ^{13}C shifts for resolving the structure (Fig. 1) (18, 19). They are an accurate probe of the secondary fields induced by the aromatic rings. The magnitude of the aggregation shifts for chlorins **1** and **2** (*cf.* Fig. 1 and Table 1) are very similar, which indicates that the pattern of stacking and the stacking motif is similar for both **1** and **2** in the solid, despite a pronounced difference at the 3^1 side chain, OH with H-bonding capability for compound **1**, and a methoxy functionality for compound **2**. The importance of the hydrogen bond has been questioned before, because extended stacks were found for simplified artificial BChl mimics due to packing by hydrophobic interactions without hydrogen bonding (20). The absence of the −OH resonance in the data of compound **1** is well in line with studies on Mg-chlorin aggregates of biological origin and semisynthetic Cd-chlorin derivatives. Apparently the −OCH3 behaves in a similar way, due to unfavorable cross-polarization (CP)-MAS properties, corroborating a similar role for the −OCH3 in compound **2** compared with the −OH moiety in **1**.

To explain the aggregation shift patterns, structural models of coordinating chlorins for **1** and **2** were built based on previously published AFM and STM data in Hyperchem 7 (13, 14). The first is the parallel stack model in which the arrangement of the chlorin cores is directed by the coordination of hydroxyl or methoxy groups to the zinc ions, and the alkyl chains of one stack are all arranged in the same direction (Fig. 3*A*), whereas the second is the antiparallel monomer stack model in which the alkyl chains of neighboring chlorins are oriented in opposite directions (Fig. 3*B*) (21). These models have been selected because compound **1** is shown to form rod like aggregates, which are thought to be built from the parallel stack motif. Compound **2**, however, has been shown to aggregate with either the antiparallel stack motif or the parallel stack motif. To simplify the quantum mechanical calculations, the 17–3,5-bis-dodecyloxybenzylalcohol tail has been replaced by a 17-methyl group and the 8-ethyl is replaced by an 8-methyl group.

For chlorins **1** and **2**, an initial parallel stack model with 6 molecules each was constructed and optimized using molecular mechanics with an MM+ force field. To investigate the possibility of H-bonding between stacks, larger aggregates of **1** were built by optimizing multiple stacks placed together with their

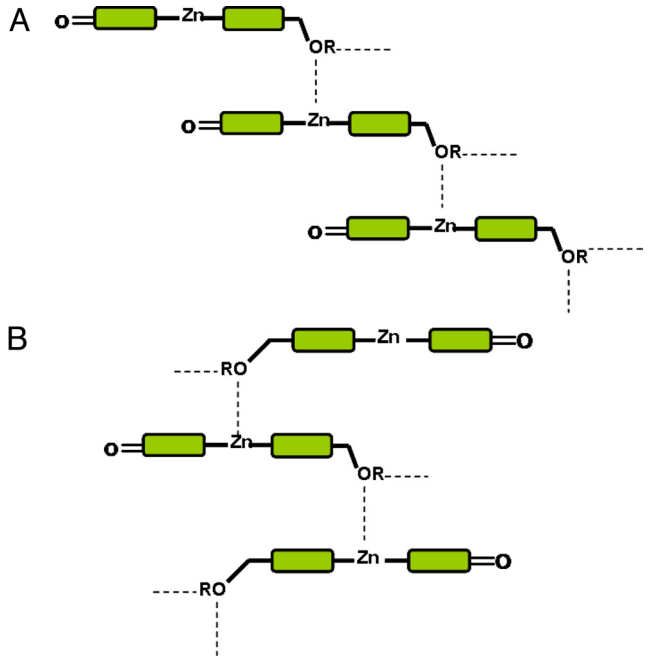

Fig. 3. Schematic representation of the models used for ring-current shift calculations. (*A*) is the parallel-stack model and (*B*) is the antiparallel stack model.

3^1-OH group of one stack within H-bonding distance of the 13^1C═O of the adjacent stack. In this way a twenty four molecule aggregate of 4 hexamer stacks was optimized for chlorin **1**. The interstack H-bond network remained intact on optimization. Due to the presence of the methoxy functionality at 3^1 in chlorin **2**, H-bonding is not possible and a single parallel stack of 12 chlorin **2** molecules was optimized. This single parallel stack for compound **2** was energetically stable. Likewise, to optimize the antiparallel stack model for **1** and **2**, a single stack of 6 molecules each was constructed. Optimization revealed that these structures are unstable as single stacks. A second 6 molecule stack was added for both **1** and **2** in the interstack H-bonding arrangement for compound **1** and with the methoxy functionalities pointing toward the 13^1C═O of the adjacent stack for compound **2**. On optimization, energetically stable aggregates were obtained for both compounds. This confirms that a stabilization mechanism is in operation to promote aggregation. To determine the factor leading to this stabilization, various contributions to the total energy for a single stack and 2 stack aggregate of compounds **1** and **2** are listed in Table S1. It was found that although the electrostatic contribution to the total energy is the most dominant, it increases linearly with aggregation. Hence, it does not contribute to the stabilization of the aggregates. There is no contribution at all from H-bonding to the stabilization of compound **2**. This is to be expected because there is no H-bonding functionality present at 3^1. Interestingly, for compound **1** there is also no contribution from H-bonding to the total energy. However, both for compounds **1** and **2**, the contribution from the nonbonding interactions or the van der Waals interaction increases nonlinearly with aggregation i.e., its contribution increases ≈4 to 5 times on going from a single stack to a 2 stack aggregate. This nonbonding energy corresponds to the stabilization from increased π–π stacking on going from a single to multiple stacks (can be seen in Fig. 4*A*). As a result, for the antiparallel stack model both for compounds **1** and **2**, the increased π–π overlap on increased aggregate size leads to an energetically cooperative stabilization mechanism, in an extended space filling structure. Under different sample

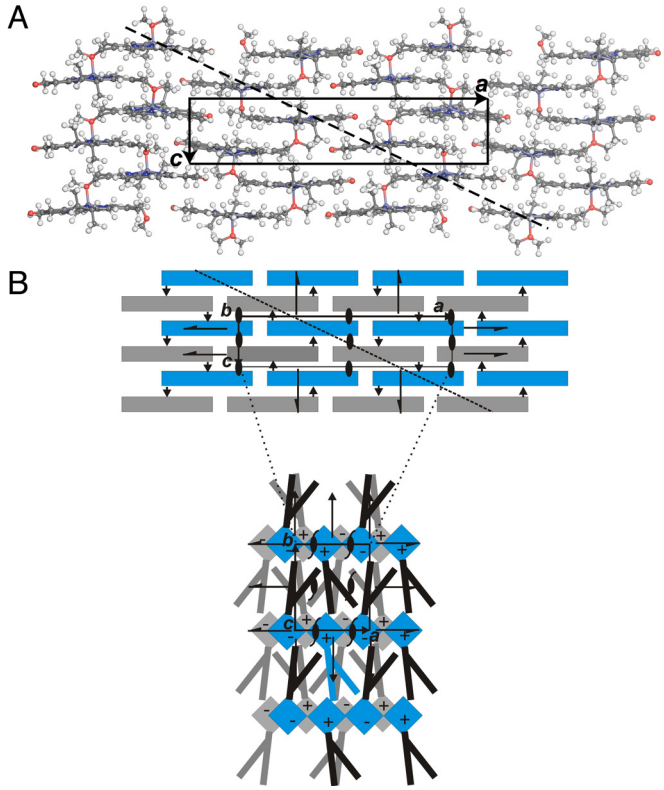

Fig. 4. Proposed 3-dimensional packing of chlorin **2** in an alternating antiparallel π-stack arrangement: (*A*) Antiparallel stack model of **2** from MM+ calculations with approximate unit cell. (*B*) Schematic representation of a possible packing matching the model and the X-ray data (see Table 3 and *Results and Discussion*) in projections along *b* (*Upper*) and *c* (*Lower*) with unit cell axes *a*–*c*. The arrows and +/− signs, respectively, show the direction of the O—Zn coordinative bond within an individual π-stack. Additionally, the symmetry elements for this hypothetical packing (space group $P2_122_1$) are shown. The orientation of the chains is arbitrary, but consistent with the proposed symmetry. The dashed line indicates a lattice plane parallel to (201), which is comparatively densely occupied by Zn atoms in this model.

preparation conditions, other arrangements could be feasible that also involve hydrogen-bonding between the stacks. Such phenomena of polymorphism are well-known for organic pigments, e.g., in the structurally related phthalocyanine pigments (22). These aggregates were further extended to 4 stacks as shown in Fig. 4*A* for chlorin **2**. ^{1}H ring-current shifts were calculated for chlorins **1** and **2** in the parallel (Fig. S2) and antiparallel (Fig. 1) stack models and are listed in Table 2.

From the differences between the experimental and the calculated ring current shifts for the 4 models (Table S2) it is clear that the aggregation shifts of chlorin **2** are in very good quantitative agreement [Table S2, $\Delta\sigma^H_{i,2} - \Delta\sigma^H_{2,\mathrm{calc}}$ (A) values] with the calculated ring-current shifts for the antiparallel stack arrangement. In contrast, the calculated ring-current shifts for **1** are in semiquantitative agreement with the observed aggregation shifts for the antiparallel stack model although they reproduce the essential features, in particular the combination of very strong aggregation shifts in the 3-CH_2 region and significant 12-CH_3 shifts. We also modeled aggregates of **1** in the closed-dimer model (Fig. S3), which has been discussed in the literature (15, 21). Ring-current shift calculations revealed a substantial mismatch (Fig. S4 and Table S3) allowing us to eliminate this model. It is also known that compounds **1** and **2** in non polar solvents (14, 23) show an aggregate bathochromic shift of the Q_y bands of ≈80–100 nm, and such shifts are not possible for

Table 2. Calculated ring current shifts $\Delta\sigma^H_{\mathrm{calc}}$ (in parts per million) for chlorins 1 and 2, each in the parallel stack (P) and antiparallel stack (A) models.

Position	$\Delta\sigma^H_{1,\mathrm{calc}}$ (P)	$\Delta\sigma^H_{2,\mathrm{calc}}$ (P)	$\Delta\sigma^H_{1,\mathrm{calc}}$ (A)	$\Delta\sigma^H_{2,\mathrm{calc}}$ (A)
5	−2.0	−1.8	−4.2	−4.3
10	−0.3	−0.2	1.5	0.3
17	2.1	−0.1	1.1	−0.2
18	1.3	−0.3	1.1	−0.1
20	−0.6	−0.1	0.7	−1.2
2^1	−2.9	−2.7	−5.5	−5.0
3^1	−3.7	−4.9	−6.0	−8.0
7^1	0.4	0.0	−0.7	−0.3
8^1	0.4	0.4	1.3	1.4
12^1	−3.3	−2.5	−4.8	−5.2
13^2	−0.5	−3.3	1.7	0.2
17^1	0.9	−0.1	1.6	−0.1
18^1	1.2	0.2	1.5	0.1

dimers. Because similar solvent combinations are used to obtain solid aggregates, closed-dimers are unlikely.

The magnitude of the aggregation shifts observed for the protons 12^1 for both compounds **1** and **2** precludes their existence as individual 1-dimensional π-stacks in the solid-state. This is because in a single antiparallel stack there is no significant ring overlap in the region of 12^1-CH_3 that could cause such a strong upfield shift. Overlap with chlorins from adjacent stacks is thus essential.

The alkyl tails constitute a factor that is important for the supramolecular organization of the 1D π-stacks. Chlorin **2** forms extensive lamellae of π-stacks on an atomically flat HOPG surface, as has been shown by the STM technique. On HOPG this arrangement is most probably favored by the strong intermolecular interaction of alkyl chains with graphite. Probably the interdigitation of tails between adjoining stacks plays an important role in stabilizing the extended lamellar structure that is observed on surfaces, in contrast with the extended H-bonding in the natural BChl stacks.

To gain further insight into how these alkyl chains influence the 3D packing of π-stacked chlorin **2** in the solid state, X-ray powder diffraction was measured at ambient temperature and at 80 °C and the results are shown in Fig. 5. Both diffraction patterns show nonequidistant and very sharp reflections in the small and wide angle regions, which confirm a highly ordered 3-dimensional arrangement of the dyes in these phases. In addition, the wide angle scattering at 80 °C shows a diffuse part with its maximum at ≈4.5 Å ($2\theta \approx 20°$), which could be

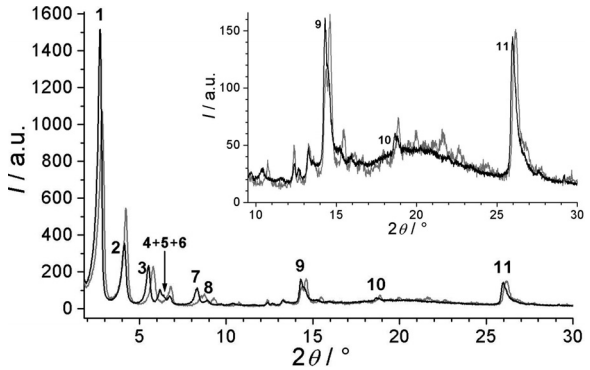

Fig. 5. X-ray diffraction pattern of **2** at ambient temperature (gray lines) and at 80 °C on heating (black lines). *Inset* shows an enlarged plot of the wide angle range; numbers indicate the reflection numbers for the pattern at 80 °C used in Table 3.

Table 3. Indexing of the small angle reflections in the powder X-ray diffraction pattern of chlorin 2 at 80°C on a 2-dimensional rectangular lattice with lattice constants a = 28.6 Å and b = 32.3 Å (the 3 strongest wide angle reflections are also shown) and comparison of the experimental (d_{obs}) and calculated (d_{calc}) d values; $hk(l)$: assigned indices (third direction c = 6.8 Å for an assumed orthorhombic unit cell matching the model considerations, space group $P2_122_1$, reflections $h00$ observed for $h = 2n$ and $00l$ for $l = 2n$ (*Results and Discussion* and Fig. 5); $d_{obs} - d_{calc}$ (Å): difference between observed and calculated parameter

Reflection no.	2θ, °	d_{obs}, Å	$hk(l)$	d_{calc}, Å	$d_{obs} - d_{calc}$, Å
1	2.73	32.4	01	32.3	0.1
2	4.11	21.5	11	21.4	0.1
3	5.51	16.0	02	16.1	−0.1
4	6.16	14.3	20	14.3	0.0
5	6.40	13.8	12	14.0	−0.2
6	6.74	13.1	21	13.1	0.0
7	8.30	10.6	22	10.7	−0.1
8	8.89	9.9	13	10.1	−0.2
9	14.4	6.2	(201	6.1	0.1)
10	18.7	4.7	(421	4.7	0.0)
11	26.0	3.4	(002	3.4	0.0)

attributed to a partially liquid-like packing of the chains. The small-angle reflections at 80 °C may be indexed with satisfactory accuracy on a primitive 2-dimensional rectangular grid with lattice constants a = 28.6 Å and b = 32.3 Å (*cf.* experimental and calculated d spacings in Table 3). The 3 strongest reflections in the wide-angle region are also numbered (reflections 9–11). The sharp peak at $2\theta = 26°$ (reflection 11) indicates a definite long-range order in the structure of the chlorin **2** with intervals of 3.4 Å. This value is characteristic of densely π-stacked dyes and delivers the interplanar distance of the chlorins in the direction perpendicular to the 2-dimensional cell. This assumption is supported by the literature known π - π distances in crystals of stacked zinc porphyrins (3.46 Å) (24, 25).

A comparison with the dimensions measured for the packing obtained from the MM+ optimized antiparallel stack model shows, that twice the distance between the chlorin **2** rings along the stacking direction is a periodic one and can be considered as the third dimension $h = d_{(\text{reflection } 11)} = 6.8$ Å in an orthorhombic 3D unit cell with a volume of $V_E = a \times b \times h = 6.28$ nm^3. However, 1 molecule of **2** in the crystalline state has an approximate volume of 1.47 nm^3 estimated according to the volume increment method of Immirzi and Perini (26). Thus, the unit cell should contain 4 molecules of chlorin **2** with a molecular volume of 1.57 nm^3, a reasonable value for the less dense phase at 80 °C, which is also consistent with the packing model. The 3D interpretation is further supported by the strong intensity of reflection 9. Using the lattice parameters from the NMR models, it may be indexed 201, and in the packing model, the Zn atoms occupy this lattice plane comparatively densely. A possible space group consistent with these considerations would be $P2_122_1$. Fig. 4 shows the antiparallel stack model as derived from NMR studies and MM+ calculations and a schematic depiction of the corresponding 3D packing mode that was derived from the XRD data collected at 80°. It is not possible to uniquely index the XRD pattern at ambient temperature. As can be seen in Fig. 5, however, the strongest reflections are only slightly changed in position and intensity (reflections 1, 2, 3, 9, 10, 11). Thus, even though the space group symmetry may be different at room temperature (most probably monoclinic or triclinic) the principal packing mode for the π-stacks appears the same as observed at 80 °C where the alkyl chains are partially molten and the material transforms into a less ordered soft crystalline phase.

Conclusions

The molecular structure and packing of self-assembled semisynthetic chlorins **1** and **2** was studied in detail in the solid-state. The experimental aggregation shifts of chlorins **1** and **2** were very well reproduced by ring-current shift calculations of the antiparallel stacking mode of the dye molecules. The local antiparallel model for **2** can be extended to a 3D periodic packing that is in line with the X-ray diffraction data for a powder-like sample at 80 °C providing a conclusive short-range structural arrangement of the dye molecules in the solid-state.

Quantum mechanical calculations allow experimental ^{1}H solid-state NMR spectra to be assigned in a quantitative manner to a specific molecular packing arrangement, starting from the chemical structure of a moderately sized molecule with different side chains that break the molecular symmetry. The combination of MAS NMR, molecular modeling and ring-current shift calculations provides a promising fingerprinting technique that can be of use in the future to investigate structure and properties of other unlabeled π-aggregated supramolecular systems of low molecular symmetry.

Materials and Methods

Zinc chlorins **1** and **2** were synthesized starting from Chl *a*, extracted from *Spirulina platensis* cyanobacteria (13, 14, 23). The intermediate compounds and the final zinc chlorin dyes **1** and **2** were purified by silica-gel column chromatography and subsequently by reverse-phase HPLC, and were characterized by solution-state ^{1}H NMR and high resolution mass spectrometry (HRMS). Analytical HPLC was performed on a system (PU 2080 PLUS) with a diode array detector (MD 2015) from JASCO equipped with a ternary gradient unit (LG 2080–02) and line degasser (DG-2080–533). Semipreparative HPLC was performed on a system (PU 2080 PLUS) with a diode array detector (UV 2077 PLUS) from JASCO. HPLC grade solvents (Rectapur) from VWR were used. Reverse phase columns obtained from Macherey-Nagel (analytical: EC 250/4.6 NUCLEODUR 100–5 C18 ec, precolumn: CC 8/4 NUCLEODUR 100–5 C18 ec; semipreparative: SP 250/21 NUCLEODUR 100–7 C18 ec, precolumn semipreparative: SP 50/21 NUCLEODUR 100–7 C18 ec) were used. Zinc chlorin **1** was eluted at 6.1 min with a flow rate of 1 mL/min with methanol/CH_2Cl_2(7:3) as eluent whereas zinc chlorin **2** was eluted at 8.9 min with a flow rate of 1 mL/min with methanol/CH_2Cl_2 (7:3). The components eluting before the characteristic retention times for **1** and **2** were discarded.

The ^{1}H NMR solution spectra were recorded at 25 °C with a 400-MHz spectrometer (Bruker). Chemical shifts (δ) are relative to TMS. The monomer ^{1}H shifts were determined in coordinating solvents, for zinc chlorin **1** ($\sigma^H_{1,liq}$) THF-d_8 and for zinc chlorin **2** ($\sigma^H_{2,liq}$) pyridine-d_5. Chlorin **2** has enhanced solubility in pyridine-d_5 and we have confirmed that the chemical shifts exhibit negligible changes compared with those in THF-d_8. Additionally, ^{1}H solution NMR in THF-d_8 + 5% CD_3OD and UV-Vis measurements in THF and THF + 5% MeOH were performed on compounds **1** and **2** to ensure that they exist as monomeric species at typical solution NMR concentrations (See *SI Text*, Figs. S5 and S6, and Table S4 for details). To prepare bulk samples for the solid-state NMR measurements, the HPLC purified dyes **1** and **2** were dissolved in a minimum amount of THF and dichloromethane, respectively, and 10 equiv. of *n*-hexane was added to each to form the aggregates in solution. The aggregates were precipitated at 0 °C, solvents were removed under vacuum with a rotary evaporator. The solids were dissolved in dioxane and the frozen solutions were lyophilized for 2–3 days to transform the aggregates into solid powders that can be packed tightly in the NMR rotors. All MAS NMR experiments were performed with a Bruker AV-750 spectrometer equipped with a 4-mm triple resonance MAS probe head, using a ^{13}C radio frequency of 188.6 MHz and a sample temperature of 298 K. A spinning frequency of 13 kHz ± 5 Hz was used for the 2D ^{1}H-^{13}C heteronuclear correlation experiments. The ^{1}H spins were decoupled during acquisition using the 2-pulse phase modulation (TPPM) scheme (27). Two-dimensional ^{1}H-^{13}C heteronuclear correlation datasets were obtained by using the frequency-switched Lee-Goldburg (FSLG) experiment, by using a short CP time of 256 μs and a ^{1}H 90° pulse of 3.1 μs (16). The ^{1}H chemical shift scale was calibrated from a FSLG spectrum of solid tyrosine·HCl salt (16). For each of 256 steps in the indirect ^{1}H dimension, 1536 ^{13}C scans were accumulated.

All geometry optimizations were done using molecular mechanics in Hyperchem 7 with an MM+ force field and used a Polak-Ribiere conjugate

gradient algorithm with a gradient convergence criterion of 0.01 kcal/mol. DFT calculations were performed using the Gaussian 03 software package (Revision D.01) and the Becke, Lee, Yang and Parr (BLYP) (28–31) exchange-correlation function, which has been used before to estimate NMR shifts for Chl systems. The 6–311++G(d,p) Gaussian basis set was used. Ring-current shifts were calculated using the Gauge-Independent Atomic Orbital (GIAO) method (32, 33). To calculate the magnetic shielding due to the local magnetic field induced by the ring current effect in the BChls, nucleus-independent chemical shift (NICS) quantum mechanical calculations were performed (34). The structural model used for the DFT calculations included the surrounding BChl molecules that are significant in causing ring-current effects.

X-ray diffraction measurements on a powder-analogue sample kept on a beryllium plate in a temperature controlled heating stage were carried out with a Guinier goniometer (Huber GmbH and Co. KG), using quartz-monochromatized $Cu_{K\alpha}$ radiation.

ACKNOWLEDGMENTS. We thank C. Erkelens, A. Lefeber and J. Hollander for their assistance and The Nederlandse Organisatie voor Wetenschappelijk Onderzoek and Stichting Nationale Computerfaciliteiten for the use of the Stichting Academisch Rekencentrum Amsterdam supercomputer facilities. This work was supported by The Netherlands Organization for Scientific Research–Division of Chemical Sciences and the Volkswagen Foundation.

1. Martinez-Planells A, et al. (2002) Determination of the topography and biometry of chlorosomes by atomic force microscopy. *Photosynth Res* 71:83–90.
2. Montano GA, et al. (2003) Characterization of Chlorobium tepidum chlorosomes: A calculation of bacteriochlorophyll *c* per chlorosome and oligomer modeling. *Biophys J* 85:2560–2565.
3. Saga Y, Shibata Y, Ltoh S, Tamiaki H (2007) Direct counting of submicrometer-sized photosynthetic apparatus dispersed in medium at cryogenic temperature by confocal laser fluorescence microscopy: Estimation of the number of bacteriochlorophyll c in single light-harvesting antenna complexes chlorosomes of green photosynthetic bacteria. *J Phys Chem B* 111:12605–12609.
4. Brune DC, et al. (1987) Antenna organization in green photosynthetic bacteria. 2. Excitation transfer in detached and membrane-bound chlorosomes from Chloroflexus aurantiacus. *Biochemistry* 26:8652–8658.
5. Savikhin S, et al. (1995) Ultrafast energy-transfer in light-harvesting chlorosomes from the green sulfur bacterium Chlorobium tepidum. *Chem Phys* 194:245–258.
6. Prokhorenko VI, Steensgaard DB, Holzwarth AR (2003) Exciton theory for supramolecular chlorosomal aggregates: 1. Aggregate size dependence of the linear spectra. *Biophys J* 85:3173–3186.
7. Tamiaki H, Amakawa M, Holzwarth AR, Schaffner, K (1995) in *Photosynthesis: From Light to Biosphere*, ed Mathis P (Kluwer, Dordrecht, The Netherlands), Vol 1, pp 61–64.
8. Scholes GD, Rumbles G (2006) Excitons in nanoscale systems. *Nat Mater* 5:683–696.
9. Smith KM, Kehres LA, Fajer J (1983) Aggregation of the bacteriochlorophylls c, d, and e. Models for the antenna chlorophylls of green and brown photosynthetic bacteria. *J Am Chem Soc* 105:1387–1389.
10. Brune DC, Nozawa T, Blankenship RE (1987) Antenna organization in green photosynthetic bacteria. 1. Oligomeric bacteriochlorophyll c as a model for the 740 nm absorbing bacteriochlorophyll c in Chloroflexus aurantiacus chlorosomes. *Biochemistry* 26:8644–8652.
11. Balaban TS, et al. (1995) CP-MAS ^{13}C-NMR dipolar correlation spectroscopy of ^{13}C-enriched chlorosomes and isolated bacteriochlorophyll-*c* aggregates of Chlorobium tepidum: The self-organization of pigments is the main structural feature of chlorosomes. *Biochemistry* 34:15259–15266.
12. Tamiaki H, Holzwarth AR, Schaffner K (1992) A synthetic zinc chlorin aggregate as a model for the supramolecular antenna complexes in the chlorosomes of green bacteria. *J Photochem Photobiol B* 15:355–360.
13. Huber V, Katterle M, Lysetska M, Würthner F (2005) Reversible self-organization of semisynthetic zinc chlorins into well-defined rod antennae. *Angewandte Chemie-International Edition* 44:3147–3151.
14. Huber V, Lysetska M, Würthner F (2007) Self-assembled single- and double-stack pi-aggregates of chlorophyll derivatives on highly ordered pyrolytic graphite. *Small* 3:1007–1014.
15. Nozawa T, et al. (1994) Structures of chlorosomes and aggregated BChl *c* in Chlorobium tepidum from solid-state high-resolution CP-MAS ^{13}C NMR. *Photosynth Res* 41:211–223.
16. van Rossum BJ, Förster H, de Groot HJM (1997) High-field and high-speed CP-MAS ^{13}C NMR heteronuclear dipolar-correlation spectroscopy of solids with frequency-switched Lee-Goldburg homonuclear decoupling. *J Magn Reson* 124:516–519.
17. van Rossum BJ, et al. (2001) A refined model of the chlorosomal antennae of the green bacterium Chlorobium tepidum from proton chemical shift constraints obtained with high-field 2-D and 3-D MAS NMR dipolar correlation spectroscopy. *Biochemistry* 40:1587–1595.
18. de Boer I, et al. (2003) MAS NMR structure of a microcrystalline Cd-bacteriochlorophyll d analogue. *J Am Chem Soc* 125:13374–13375.
19. de Boer I, et al. (2004) MAS NMR structures of aggregated cadmium chlorins reveal molecular control of self-assembly of chlorosomal bacteriochlorophylls. *J Phys Chem B* 108:16556–16566.
20. Jochum T, et al. (2008) The supramolecular organization of self-assembling chlorosomal bacteriochlorophyll c, d, or e mimics. *Proc Natl Acad Sci USA* 105:12736–12741.
21. Holzwarth AR, Schaffner K (1994) On the structure of bacteriochlorophyll molecular aggregates in the chlorosomes of green bacteria—a molecular modeling study. *Photosynth Res* 41:225–233.
22. Herbst W, Hunger, K (1997) *Industrial Organic Pigments*, *Production*, *Properties*, *Applications* (Wiley, Weinheim, Germany).
23. Huber V, Sengupta S, Würthner F (2008) Structure-property relationships for self-assembled zinc chlorin light-harvesting dye aggregates. *Chem A Eur J* 14:7791–7807.
24. Balaban TS, et al. (2005) Structural characterization of artificial self-assembling porphyrins that mimic the natural chlorosomal Bacteriochlorophylls c, d, and e. *Chem A Eur J* 11:2268–2275.
25. Manickam M, et al. (2001) The first hexagonal columnar discotic liquid crystalline carbazole derivatives induced by noncovalent pi-pi interactions. *J Mater Chem* 11:2790–2800.
26. Immirzi A, Perini B (1977) Prediction of density in organic-crystals. *Acta Crystallogr A* 33:216–218.
27. Bennett AE, et al. (1995) Heteronuclear decoupling in rotating solids. *J Chem Phys* 103:6951–6958.
28. Frisch MJ, et al. (2004) Gaussian 03, RevisionD.01. (Gaussian, Wallingford CT).
29. Becke AD (1986) Density functional calculations of molecular bond energies. *J Chem Phys* 84:4524–4529.
30. Lee CT, Yang WT, Parr RG (1988) Development of the colle-salvetti correlation-energy formula into a functional of the electron-density. *Phys Rev B* 37:785–789.
31. Facelli JC (1998) Density functional theory calculations of the structure and the ^{15}N and ^{13}C chemical shifts of methyl bacteriopheophorbide a and bacteriochlorophyll a. *J Phys Chem B* 102:2111–2116.
32. Ditchfield R (1974) Self-consistent perturbation-theory of diamagnetism. 1. Gauge-invariant LCAO method for NMR chemical-shifts. *Mol Phys* 27:789–807.
33. Wolinski K, Hinton JF, Pulay P (1990) Efficient implementation of the gauge-independent atomic orbital method for chemical-shift calculations. *J Am Chem Soc* 112:8251–8260.
34. Chen ZF, et al. (2005) Nucleus-independent chemical shifts (NICS) as an aromaticity criterion. *Chem Rev* 105:3842–3888.